Type of contribution:
Editorial
▶ Research Paper
Case Study
Review Paper
Scientific Data
Report of Tech. Application

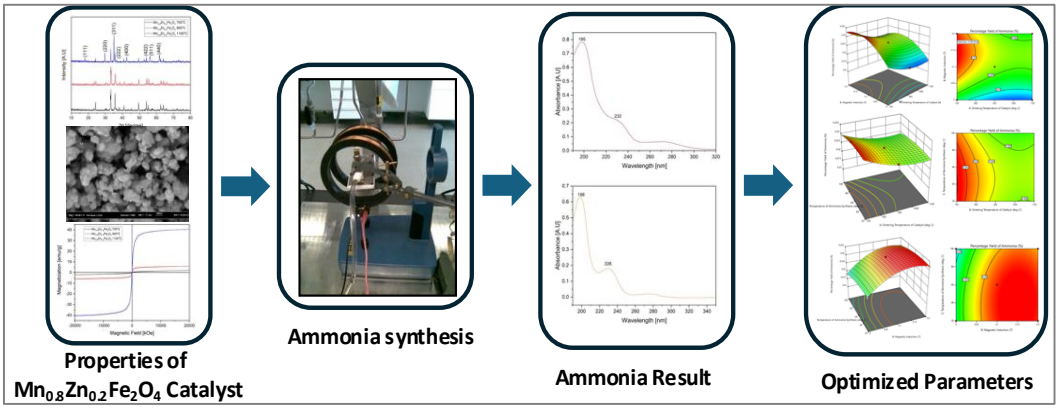
mesi
e-issn. 2798-5245

Mechanical Engineering for Society and Industry
Vol. 5, No. 2 (2025) pp 303-318
https://doi.org/10.31603/mesi.13408

Application of response surface methodology (RSM) and central composite design (CCD) to optimize of green ammonia production using magnetic induction method (MIM) and nanocatalysts

Poppy Puspitasari[1,2]*, Nandang Mufti[2,3], Ahmad Atif Fikri[1], Deny Yudo Wahyudi[4], Maizatul Shima binti Shaharun[5,6], Anisa Ur Rahmah[7], Diki Dwi Pramono[1,2]

[1] Department of Mechanical and Industrial Engineering, Universitas Negeri Malang, Malang 65145, **Indonesia**
[2] Nanomaterials Engineering Research Center, Universitas Negeri Malang, Malang 65145, **Indonesia**
[3] Department of Physical Science of Materials, Universitas Negeri Malang, Malang 65145, **Indonesia**
[4] Department of History, Universitas Negeri Malang, Malang 65145, **Indonesia**
[5] CO_2 Research Center (CO_2RES), Institute of Contaminant Management, Universiti Teknologi PETRONAS, **Malaysia**
[6] Department of Fundamental and Applied Science, Universiti Teknologi PETRONAS, **Malaysia**
[7] Department of Chemical Engineering, Universitas Muhammadiyah Surakarta, Sukoharjo 57169, **Indonesia**
✉ poppy@um.ac.id



Highlights:

- Investigation of $Mn_{0.8}Zn_{0.2}Fe_2O_4$ catalyst for ammonia synthesis, focusing on sintering temperatures, magnetic induction, and calcination temperatures to improve synthesis efficiency.
- The $Mn_{0.8}Zn_{0.2}Fe_2O_4$ catalyst has sub-round morphology with high sphericity and a tendency for agglomeration. The catalyst exhibits ferrimagnetic characteristics at 700 °C and 900 °C sintering temperatures, and ferromagnetic characteristics at 1100 °C.
- Successful synthesis of ammonia in forms of NH_4OH and $(NH_4)_2SO_4$ using the $Mn_{0.8}Zn_{0.2}Fe_2O_4$ catalyst via the Helmholtz coil method.
- Response Surface Methodology (RSM) and Central Composite Design (CCD) were used to optimize the synthesis process, achieving an R^2 value of 99.73%, indicating model accuracy.
- Best synthesis conditions include a sintering temperature of 700 °C, magnetic induction of 0.14 T, and an ammonia synthesis temperature of 28 °C. Validation shows high correlation and low residuals between predicted and experimental responses, confirming the quadratic regression model's reliability and accuracy.

Article info
Submitted: 2025-04-16
Revised: 2025-06-28
Accepted: 2025-06-30

This work is licensed under a Creative Commons Attribution-NonCommercial 4.0 International License

Publisher
Universitas Muhammadiyah Magelang

Abstract

Ammonia synthesis in conventional industrial plants typically employs fused iron-based catalysts under harsh conditions (temperatures of 400–700 °C and pressures exceeding 300 atm), resulting in significant energy consumption. This study investigates the potential of using a $Mn_{0.8}Zn_{0.2}Fe_2O_4$

catalyst, synthesized under varying sintering temperatures and magnetic field inductions, to enable ammonia synthesis under milder conditions. Additionally, process optimization was carried out using Response Surface Methodology (RSM) and Central Composite Design (CCD). Catalyst characterization results indicate that the crystallite size of $Mn_{0.8}Zn_{0.2}Fe_2O_4$ increases with higher sintering temperatures. The catalyst exhibits a near-spherical morphology with notable agglomeration. Magnetic property analysis shows that samples sintered at 700 °C and 900 °C display ferrimagnetic behavior, while the sample sintered at 1100 °C exhibits ferromagnetic characteristics. Temperature-Programmed Reduction (TPR) revealed a maximum reduction peak at 788 °C for the catalyst sintered at 1100 °C, indicating enhanced reducibility. Ammonia formation was successfully achieved using a Helmholtz coil-assisted synthesis method, where the produced ammonia was captured in acidic and basic media in the form of NH_4OH and $(NH_4)_2SO_4$, confirming the catalytic activity of $Mn_{0.8}Zn_{0.2}Fe_2O_4$. The RSM model demonstrated high accuracy with an R^2 value of 99.73%, and residual analysis confirmed normal distribution, validating model assumptions. The optimal synthesis parameters determined were a sintering temperature of 700 °C, magnetic induction of 0.14 T, and a reaction temperature of 28 °C. The minimal deviation between predicted and experimental responses confirms the reliability and predictive accuracy of the quadratic regression model.

Keywords: Ammonia synthesis; Nanocatalysts; MIM; RSM; CCD

1. Introduction

The synthesis of ammonia remains one of the most important industrial processes because of its use in the production of nitrogenous fertilizers that support more than seventy percent of the world population. Currently, approximately 160 million tons of ammonia is generated per year, 80% of which is used for fertilizer manufacturing [1], [2], [3]. Furthermore, ammonia is also an important industrial chemical that has various other applications such as use in refrigeration systems [4]. The predominant method of synthesizing ammonia in the industry is by using iron-based catalysts under high pressure (20-40 MPa) and high-temperature (673-873K) conditions [5]. This method requires a considerable amount of energy [2]. Improving the catalytic activity at lower temperatures and pressures is the still the most important problem the many try to focus on to improve energy efficiency [6], [7], [8].

Catalysts used for the synthesis of ammonia have been improved in the last couple of decades. The once used iron-based catalysts have been replaced by ruthenium, which increased the yield ammonia from 20% to about 40%. The main issue preventing the adoption of these new catalysts is their high cost. For example, ruthenium is about £1596.60 per 100 g [9]. Even so, more research can be done to find other catalysts that are cheaper and more energy efficient.

Ammonia synthesis is a prime example of heterogeneous catalysis. Recent advances in nanocatalysis have demonstrated that catalytic activity, selectivity, and stability can be improved by altering the size and shape of the nanomaterials. Due to their small sized active sites, nanocatalysts provide greater surface area which enhances interaction with the reactants in both homogeneous and heterogeneous catalytic reactions [10], [11]. The size and morphology of nanocatalysts impact their surface area and thus their catalytic performance, which also determines the efficiency of environmentally benign chemical transformations enabled by these catalysts [12], [13].

Recent research has shown that permanent magnets and oscillating magnetic fields affect the green synthesis of ammonia using NH_3. The yield of ammonia is enhanced with increased magnetic induction strength and the addition of oscillating magnetic fields, indicating that magnetic fields may be vital to the efficiency of the synthesis process [5], [14]. Optimization of the synthesis process, however, is an iterative challenge involving the blending of differing conditions.

Earlier analyses focused on the impacts of catalysts, reaction temperature and pressure within the context of ammonia yield. However, the exploration of other parameters such as the impact of magnetic fields and certain catalyst compositions remains lacking. This gives the chance to improve the ammonia synthesis process by testing these uncharted parameters.

In this work, RSM (Response Surface Methodology) in combination with CCD (Central Composite Design) is applied for the determination of ammonia synthesis optimal conditions. RSM is a useful statistical method designed for the analysis and optimization of experimental results, helping in advanced modeling and verification of processes. With the application of CCD, this approach allows the assessment of the additive and interactive contributions of multiple

parameters to the ammonia yield with the expanding framework of empirical modeling aimed at advancing catalyst and process design [15], [16].

Therefore, this study is designed to investigate if ammonia synthesis may be improved by employing new catalytic materials, incorporating magnetic fields, and utilizing advanced optimization techniques. The synthesized compounds are aimed to be achieved in an economically favorable manner and with minimal detrimental effects on the environment, not only for the benefit of the fertilizer industry but also for other sectors.

2. Methods

2.1. Synthesis $Mn_{0.8}Zn_{0.2}Fe_2O_4$ Catalyst

$Mn_{0.8}Zn_{0.2}Fe_2O_4$ precursor was prepared by mixing $Mn(NO_3)_2.4H_2O$, $Zn(NO_3)_2.6H_2O$, and $Fe(NO_3)_3.9H_2O$ with 65% HNO_3. The prepared samples were stirred for 1 week and heated gradually until combustion occurred at 110 °C [17]. The samples were then dried in an oven at 110 °C for 24 hours and sintered at 700 °C, 900 °C and 1100 °C in an argon furnace for 4 hours [18]. The catalysts were analyzed for phase and crystallite size using Phillips X-ray diffraction (XRD) using Cu$K\alpha$, with λ=1.5418Å, the scanning angles (θ) were performed from 10° to 80° and the speed of the counter was 0.02°/2ϑ per min. The morphology of the catalyst was analyzed using Zeiss Supra 55/55 VP Field Emission Scanning Electron Microscope (FE-SEM) model, it was operated at 0.1kV to 30kV and magnification of 20X to 900KX. Magnetic properties were analyzed at room temperature using a Cryogen-free 3 Tesla, VersaLab™ Vibrating Sample Magnetometer (VSM). The reducibility of $Mn_{0.8}Zn_{0.2}Fe_2O_4$ catalysts were analyzed using TPD/R/O 1100, Thermo Electron Temperature Program Reduction (TPR) with Hydrogen 5% in Nitrogen and flow of 20 ccm/min, heating rate 10°/min, stop at 800 °C, hold for 15 min.

2.2. Synthesis of Ammonia

Figure 1a shows the design of ammonia synthesis using a Helmholtz coil and generator, where the Helmholtz coil and working generator are used to generate a high frequency oscillating magnetic field. The oscillating magnetic field region is located before the MIM region, as shown in **Figure 1b**. The main role of the oscillating magnetic field is to cause the N_2 and H_2 magnetic spins to rotate at high-speed following the direction of the magnetic field to weaken the reactant gas bonds. Permanent magnets are used in the MIM region with the purpose of supplying a permanent magnetic field. The formation of NH_3 occurs in this region, where the weak reactant gases that have just passed through the oscillating magnetic field will undergo electron exchange with the nanocatalyst and form NH_3 [19]. A simple glass tube was used to model the microreactor in the system. The proposed nanocatalyst is spiral-shaped to help create turbulent flow of reactant gases in the reaction area to enhance the mixing of reactant gases. The nanocatalyst is placed in the oscillating magnetic field region and magnetic induction region.

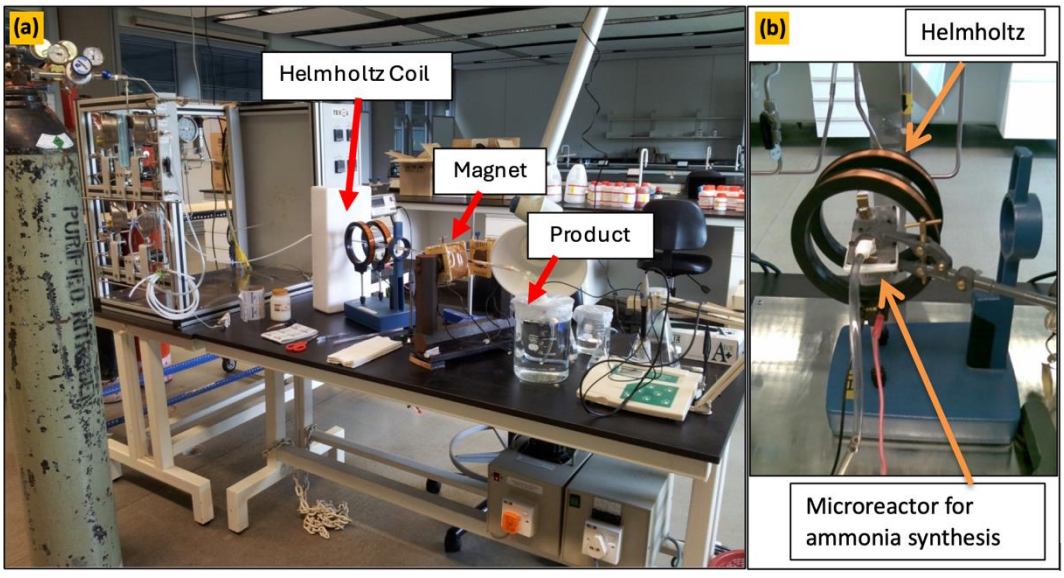


Figure 1. (a) Helmholtz microreactor design; (b) Schematic of NH_3 green synthesis using MIM

Ammonia synthesis was started by putting 0.2g of nanocatalyst into the cylinder chamber followed by turning on the MIM reactor, magnetic induction used was 0T, 0.1T and 0.2T. The ratio of N_2 and H_2 gas was 3:1 with a flow rate of 3.3 ml/min. The magnetizer was set at 10 Ampere. Reaction temperatures were carried out at 28 °C, 68 °C and 108 °C and NH_3 gas was collected for 30 minutes in 0.01M HCl. Ammonia detection was obtained using UV-Vis method, at the wavelength range of 190-320nm and the sampling interval is 0.5. Ammonia quantity analysis using Kjeldahl Method (following Eq. (1)-Eq. (5)), by diluting the gas into 5ml of 0.01M HCl which produced NH_4Cl. After that the titration process was taken using 0.01M NaOH. The amount of NH_3 produced is equal to the amount of $HCl_{reaction}$.

$$HCl_{Reaction} + NH_3 \rightarrow NH_4Cl \quad (1)$$

$$NaOH + HCl_{excess} \rightarrow NaCl + H_2O \quad (2)$$

$$HCl_{Total} = HCl_{Reaction} + HCl_{Excess} \quad (3)$$

$$\text{Amount of } HCl_{Reacted} = \text{Amount of } NH_3 \quad (4)$$

$$\text{Amount of } HCl_{Excess} = \text{Amount of } NaOH \quad (5)$$

Percentage Yield of Ammonia is calculated using Eq. (6).

$$Percentage\ Yield\ of\ Ammonia = \frac{Actual\ Yield}{Theoritical\ Yield} \times 100\% \quad (6)$$

Where to get the actual yield of ammonia adapting the reaction of the Kjeldahl method (Eq. (4)) shown in Eq. (7) below:

$$Actual\ Yield\ (from\ Kjedahl) = HCl_{Reacted} \times mol\ NH_3 \quad (7)$$

Meanwhile, to get the theoretical yield value, we must first know whether N_2 or H_2 is the limiting reagent. To determine the stoichiometric ratio of reactants using Eq. (9), because N_2 is a reaction limiter, the NH_3 yield depends on the presence of N_2, then Eq. (10) is obtained. Then the equation to find the theoretical yield is shown in Eq. (11).

$$N_2 + 3H_2 \rightarrow 2\ NH_3 \quad (8)$$

$$\frac{mol\ H_2 initial}{mol\ N_2 initial} \quad (9)$$

$$n\ NH_3 = mol\ N_2 initial \times \frac{2\ mol\ NH_3}{1\ mol\ N_2} \quad (10)$$

$$Theoritical\ Yield = n\ NH_3 \times \frac{17.03\ g\ NH_3}{1\ mol\ NH_3} \quad (11)$$

2.3. RSM Optimization of Ammonia Synthesis

For the experimental design in this study, the Central Composite Design (CCD) technique tool was used in Design Expert software version 11.1.0 because this tool has excellent capabilities for designing excellent experiments for mixtures or combinations of factors, components, and processes. Basically, researchers provide input and output variables to Design Expert RSM to generate an experimental design, so in this study, sintering temperature of catalyst (700 °C, 900 °C and 1100 °C), magnetic induction (0, 0.1 and 0.2T) and temperature of ammonia synthesis (28 °C, 68 °C and 108 °C) were used as input variables and the response variable was the percentage yield of ammonia. **Table 1** illustrates the parameter ranges used in the CCD for statistical analysis and **Table 2** shows the experimental design.

Table 1. Coded and uncoded factor levels for each input variable in the central composite design (CCD)

Input Variables	Symbol	Unit	Coded and Un-Coded Factor Level		
			-1	0	1
Sintering Temperature of Catalyst	A	°C	700	900	1100
Magnetic Induction	B	T	0	0.1	0.2
Temperature of Ammonia Synthesis	C	°C	28	68	108

3. Results and Discussion

3.1. Characterization of $Mn_{0.8}Zn_{0.2}Fe_2O_4$ Catalyst

3.1.1. Phase and Crystallite Size of $Mn_{0.8}Zn_{0.2}Fe_2O_4$ Catalyst

The XRD test on the $Mn_{0.8}Zn_{0.2}Fe_2O_4$ was carried out to identify the phase and crystallite size [20]. The crystallite size was calculated using the Scherrer, shown in Eq. (12) [21]. **Table 2** shows that the crystallite size of the $Mn_{0.8}Zn_{0.2}Fe_2O_4$ sample increases with increasing sintering temperature. Crystal growth is higher as the sintering temperature increases because the diffusion rate of atoms will increase so that the rate of crystal growth also increases and produces a larger crystallite size [22], [23]. **Figure 2** is the diffraction pattern of the $Mn_{0.8}Zn_{0.2}Fe_2O_4$ sample which shows peaks at (111), (220), (311), (222), (400), (422), (511) and (440), the characteristics of these peaks show a match with MnZn ferrite spinel (JCPDS No.74-2402). The different peak intensities at (311) are due to the sintering temperature, which causes the atoms to move out of their lattices completely. It is also speculated that Zn^{2+} ions occupy tetrahedral sites, Mn^{2+} ions occupy octahedral sites and Fe^{3+} ions are distributed in both sites [24], [25].

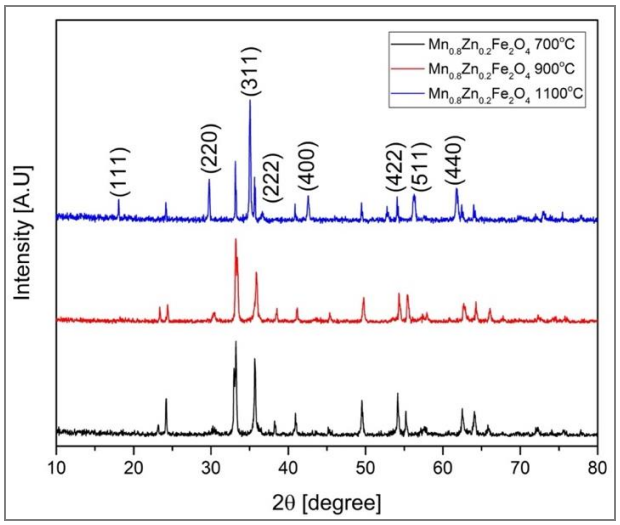


Figure 2. XRD results on $Mn_{0.8}Zn_{0.2}Fe_2O_4$ catalyst

$$d = \frac{k.\lambda}{\beta \cos \theta} \quad (12)$$

Table 2. Crystallite size of $Mn_{0.8}Zn_{0.2}Fe_2O_4$

Samples	FWHM [°2Th.]	d-spacing [Å]	Cristallite size [nm]
$Mn_{0.8}Zn_{0.2}Fe_2O_4$ 700 °C	0.39	2.70	21.10
$Mn_{0.8}Zn_{0.2}Fe_2O_4$ 900 °C	0.27	2.68	31.59
$Mn_{0.8}Zn_{0.2}Fe_2O_4$ 1100 °C	0.24	2.54	34.09

3.1.2. Morphology of $Mn_{0.8}Zn_{0.2}Fe_2O_4$ Catalyst

The analysis of morphology was carried out using an FE-SEM test. This test enabled us to determine the morphological differences of $Mn_{0.8}Zn_{0.2}Fe_2O_4$. Based on **Figure 3** shows that $Mn_{0.8}Zn_{0.2}Fe_2O_4$ has a sub-roundness morphology with high sphericity and agglomeration occurs in the sample. this is due to the nanomaterial has a large specific surface area, so it tends to be unstable and form an agglomeration state [26]. Based on **Figure 3** shows that the particle size and agglomeration of particles increases with increasing sintering temperature, this indicates that the sintering process causes the phenomenon of grain growth [27]. During the sintering process due to the heat given, the crystals that are in a particle will get bigger or grow, this is what causes the particle to grow. This event will continue to occur along with the increase in calcination temperature given. With the increasing size of the crystals in the grain, it will cause each grain to also experience growth so that the grains will be tighter [28].

3.1.3. Magnetic Properties of $Mn_{0.8}Zn_{0.2}Fe_2O_4$ Catalyst

The magnetization effect of $Mn_{0.8}Zn_{0.2}Fe_2O_4$ catalyst was tested using VSM and the test result curve is presented in **Figure 4**. Based on **Figure 4** and **Table 3**, the $Mn_{0.8}Zn_{0.2}Fe_2O_4$ sample is included in the soft magnetic category. In samples with a sintering temperature of 1100 °C has ferromagnetic characteristics [25], while in samples with temperatures of 700 °C and 900 °C has ferrimagnetic characteristics. **Table 3** shows that magnetic saturation (Ms) increases with an increase in sintering temperature. Especially, there is a significant increase in with sintering temperature which is evident from 900 °C to 1100 °C. Magnetic saturation (Ms) is mainly sensitive to the chemical composition and proximity of ferromagnetic atoms [29]. The increase in sintering temperature promotes enhanced crystallinity and grain growth, which can reduce defects and grain boundaries that act as pinning centers. This leads to an increase in the alignment of magnetic

domains and, consequently, a higher saturation magnetization (Ms). Furthermore, at elevated temperatures, the redistribution or substitution of Fe atoms within the catalyst structure may favor configurations that enhance ferromagnetic ordering [30]. In addition, the sintering temperature can affect the density, grain size, and porosity of the material, which might affect the overall magnetic properties of the material. Research conducted by Nguyen *et al*. [31] showed that if the grain size decreases, the magnetic saturation also decreases. Hence, smaller crystallite size shows lower magnetic saturation and vice versa.

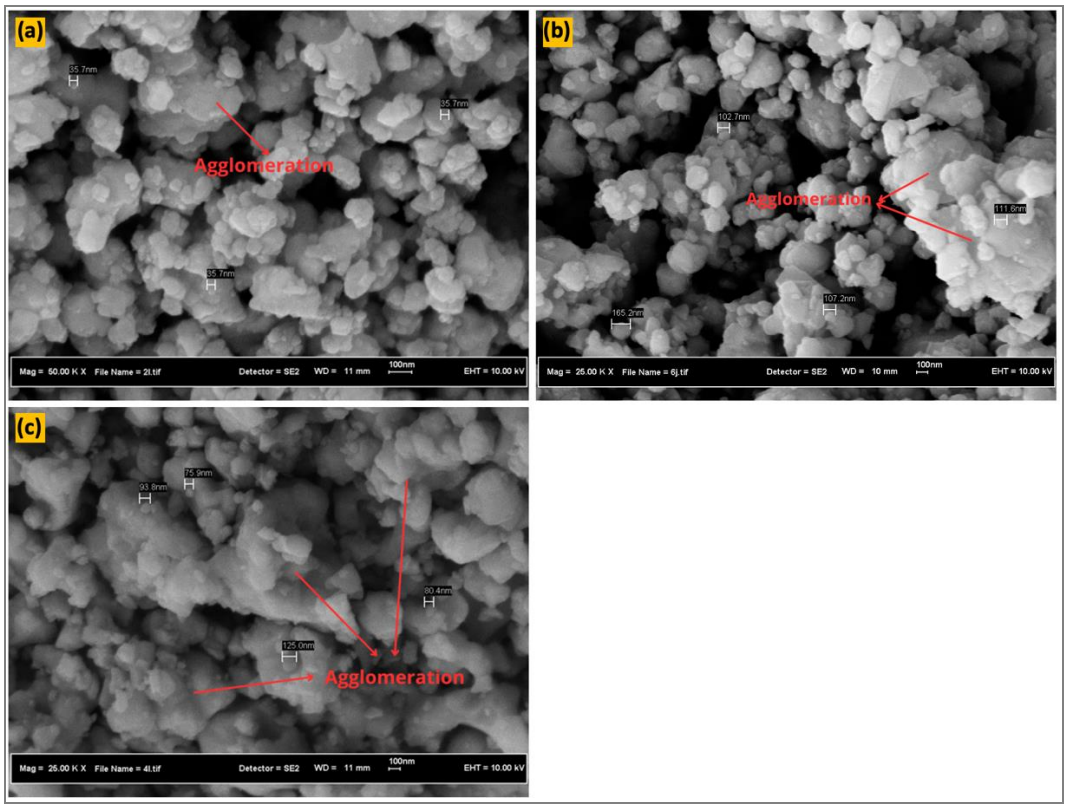


Figure 3. FE-SEM results on $Mn_{0.8}Zn_{0.2}Fe_2O_4$ catalyst sintered at: (a) 700 °C; (b) 900 °C; (c) 1100 °C

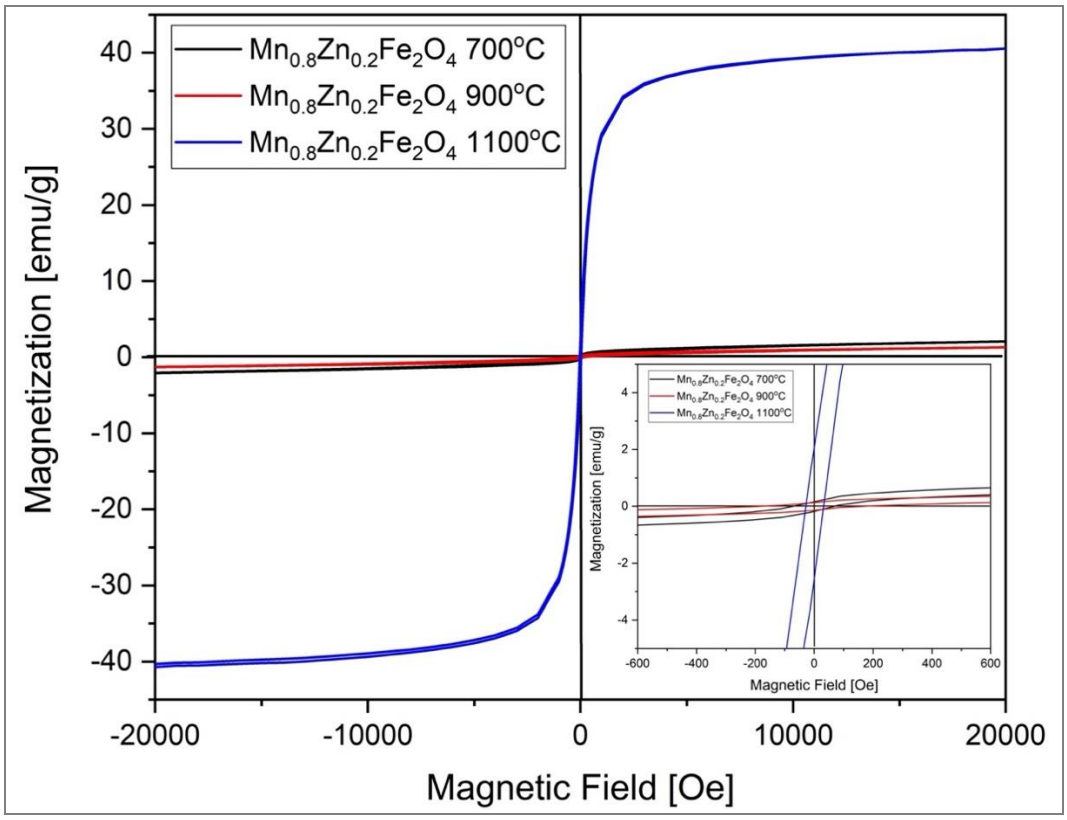


Figure 4. VSM results on $Mn_{0.8}Zn_{0.2}Fe_2O_4$ catalyst

Table 3. Hysteresis data of $Mn_{0.8}Zn_{0.2}Fe_2O_4$ catalyst

Samples	Magnetic Saturation, Ms [emu/g]	Magnetic Remanence, Mr [emu/g]	Coercivity Force, Hc [Oe]
$Mn_{0.8}Zn_{0.2}Fe_2O_4$ 700 °C	2	0.2	9
$Mn_{0.8}Zn_{0.2}Fe_2O_4$ 900 °C	5.8	1.5	14
$Mn_{0.8}Zn_{0.2}Fe_2O_4$ 1100 °C	40.3	14.9	13

3.1.4. Reducibility of $Mn_{0.8}Zn_{0.2}Fe_2O_4$ Catalyst

The reducibility of $Mn_{0.8}Zn_{0.2}Fe_2O_4$ catalysts were studied using H_2-TPR. **Figure 5** and **Table 4** reveals the H_2-TPR profiles for $Mn_{0.8}Zn_{0.2}Fe_2O_4$ with different sintering temperatures. Based on **Figure 5** and **Table 4** show that the $Mn_{0.8}Zn_{0.2}Fe_2O_4$ 700 °C, $Mn_{0.8}Zn_{0.2}Fe_2O_4$ 900 °C and $Mn_{0.8}Zn_{0.2}Fe_2O_4$ 1100 °C catalyst shows the first reduction occur at 255°C, 327°C and 346 °C for Fe_2O_3 to Fe_3O_4. It has been reported that the reduction for Fe_2O_3 to Fe_3O_4 happened at 245–360 °C [32], [33]. The second reduction peak for $Mn_{0.8}Zn_{0.2}Fe_2O_4$ is at 503 °C, 567 °C and 586 °C it can be speculated as reduction peak to MnO and FeO. It was reported that the manganese ferrite will reduce into FeO and MnO above 500 °C [34], [35]. The third reduction peak is at 776 °C, 745 °C and 788 °C which is an expected temperature for reducing all the oxide to the metallic state. As it was reported before that above 800 and 1200 °C the metallic iron expected to occur [35], [36].

The percentage hydrogen consumptions for three catalysts show that $Mn_{0.8}Zn_{0.2}Fe_2O_4$ 700 °C catalyst used most of the hydrogen gases (0.66% left). It is followed by $Mn_{0.8}Zn_{0.2}Fe_2O_4$ 900 °C catalyst which only left 0.99% hydrogen gases at the end of reduction. The $Mn_{0.8}Zn_{0.2}Fe_2O_4$ 1100 °C catalyst has 8.19% hydrogen consumption at the last reduction. The percentage hydrogen usage for the reduction depends on the crystallite size of the particle, as small particle size and crystallites can improve hydrogen storage properties [37]. This is because smaller particles and grain boundaries create pathways for hydrogen transportation [38].

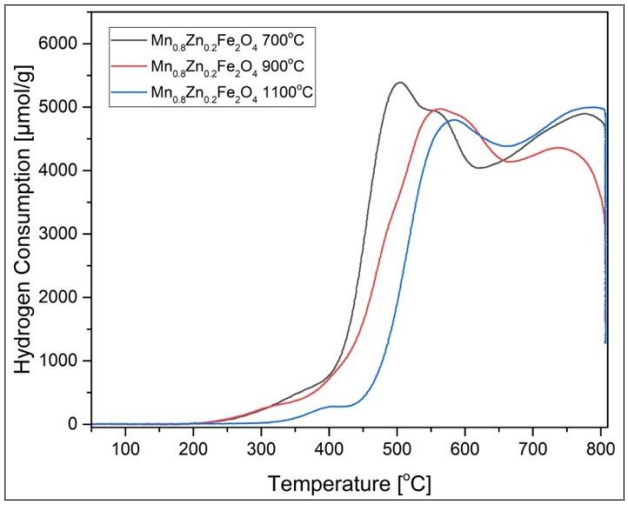


Figure 5. TPR profiles for $Mn_{0.8}Zn_{0.2}Fe_2O_4$ catalyst

Table 4. Percentage hydrogen consumption in TPR process for $Mn_{0.8}Zn_{0.2}Fe_2O_4$ catalyst

$Mn_{0.8}Zn_{0.2}Fe_2O_4$ 700 °C		$Mn_{0.8}Zn_{0.2}Fe_2O_4$ 900 °C		$Mn_{0.8}Zn_{0.2}Fe_2O_4$ 1100 °C	
Temp. [°C]	H [µmole/g]	Temp. [°C]	H [µmole/g]	Temp. [°C]	H [µmole/g]
255	625.33	327	511.07	346	241.34
503	1596.22	567	1138.76	586	1092.18
617	785.98	670	899.66	662	1057.10
776	887.01	745	682.62	788	958.54

3.2. Ammonia Production Result

Ammonia synthesis was analyzed using four methods. UV Visible spectrophotometry (UV-VIS) was used for qualitative analysis. **Figure 6a** shows the results of ammonia detection using UV-VIS spectrometry. The main peak is at 195nm which corresponds to the characteristic absorption of N-H bond standards [39]. It has been studied that saturated compounds containing atoms with lone pairs (non-bonding electrons) such as alcohols, ammonia, amines, and others are able to show a non-bonding to antibonding transition. The energy required for this transition is lower than the bonding-antibonding transition energy.

The UV-Vis results for ammonia detection using sulfuric acid base are presented in **Figure 6b**. The highest peak is 198nm wavelength and other peaks appear at 228nm and 278nm wavelengths which correspond to N-H bonding peaks [39].

3.3. Central Composite Design Model and Analysis

The 3-factor CCD design matrix generated by the software and the experimental data obtained in the ammonia synthesis process are summarized in **Table 5**.

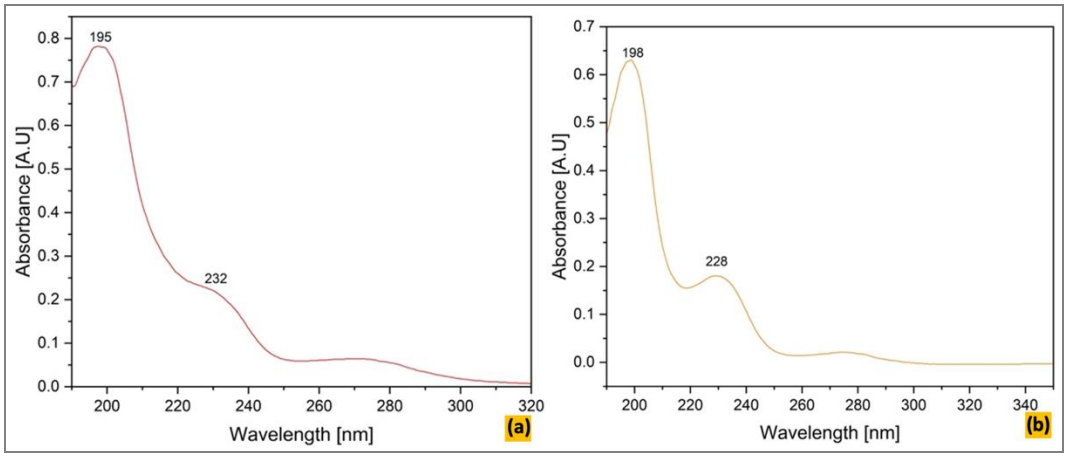


Figure 6. UV-VIS results for ammonia detection using $Mn_{0.8}Zn_{0.2}Fe_2O_4$ in the form of: (a) NH_4OH (b) $(NH_4)_2SO_4$

Table 5. Design matrix for ammonia production factors and corresponding responses of the experiment

Run	Input Parameters			Output Parameters
	Sintering Temperature of Catalyst [°C]	Magnetic Induction [T]	Temperature of Ammonia Synthesis [°C]	Percentage Yield of Ammonia [%]
1	900	0.1	68	0.0267454
2	1100	0.1	68	0.0257183
3	900	0.1	28	0.0267321
4	900	0.1	68	0.0263391
5	900	0.2	68	0.0261652
6	900	0.0	68	0.0168144
7	700	0.1	68	0.0331717
8	900	0.1	68	0.0265454
9	700	0.0	28	0.0219418
10	900	0.1	68	0.0263454
11	1100	0.0	108	0.0142374
12	700	0.2	108	0.0297754
13	900	0.1	108	0.0240759
14	900	0.1	68	0.0266321
15	1100	0.2	28	0.0240086

A quadratic model relating Percentage Yield of Ammonia and independent parameters was selected by the CCD (Table 5) and described in terms of coded parameters with a second-order polynomial equation as given in Eq. (13).

$$Y = 0.0266 - 0.0037A + 0.0047B - 0.0013C - 0.0008AB + 0.0003AC + 0.0004BC + 0.0026A^2 - 0.0053B^2 - 0.0014C^2 \quad (13)$$

The results of the analysis of variance (ANOVA) for the model are presented in Table 6 and Table 7. The F value of the developed model was found to be 14.84, which illustrates that the model is statistically significant. The large F value may occur due to noise and there is only a 0.01% chance. The "Prob > F" value was seen to be less than 0.0500, which indicates that the model is significant. Model terms A, B, C, AB, AC, BC, A^2, B^2 and C^2 were found to be significant for Percentage

Table 6. Design matrix for ammonia production factors and corresponding responses of the experiment

Source	Sum of Squares	df	Mean Square	F-value	p-value	Remarks
Model	0.0003	9	0.0000	436.73	< 0.0001	significant
A-Sintering Temperature of Catalyst	0.0000	1	0.0000	364.17	< 0.0001	
B-Magnetic Induction	0.0000	1	0.0000	573.18	< 0.0001	
C-Temperature of Ammonia Synthesis	3.528E-06	1	3.528E-06	46.25	0.0010	
AB	9.491E-07	1	9.491E-07	12.44	0.0168	
AC	1.002E-07	1	1.002E-07	1.31	0.3035	
BC	1.717E-07	1	1.717E-07	2.25	0.1938	
A^2	0.0000	1	0.0000	238.87	< 0.0001	
B^2	0.0001	1	0.0001	968.95	< 0.0001	
C^2	5.138E-06	1	5.138E-06	67.36	0.0004	
Residual	3.814E-07	5	7.627E-08			
Lack of Fit	2.542E-07	1	2.542E-07	7.99	0.0475	significant
Pure Error	1.272E-07	4	3.180E-08			
Cor Total	0.0003	14				

Table 7. Model statistics of the developed model

R^2	0.9973
Adjusted R^2	0.9938
Predicted R^2	0.8091
Adeq Precision	56.4086
Std. Dev.	0.0016
Mean	0.0250
C.V. %	1.10

Yield of Ammonia. The p value for the observed models was <0.001, indicating the level of significance for the developed models. If the p value is greater than 0.10, then the model terms are not significant [40]. **Table 6**, the lack of fit F-value of 0.0475 showed the lack of fit is not significant relative to the pure error. Nonsignificant lack of fit, however, is good because the model is geared toward perfect fitness [41].

Other statistical parameters such as coefficient of determination or R^2, adjusted R^2 (R^2_{adj}), predicted R^2 (R^2_{pred}), coefficient of variation (CV%), etc. (as shown in **Table 9**), were also used to evaluate the competency of the developed model [41]. The R^2 and R^2_{adj} values for Percentage Yield of Ammonia were found to be 0.9973 and 0.9938. The standard deviation for the model was also found to be small, at 0.0016. R^2 values close to one and smaller standard deviation values indicate better predictions from the developed model [40], [42]. The value of R^2_{pred} showed a difference value of not more than 0.2 with R^2_{adj} which means that the value is very appropriate. "Adeq Precision" determines the signal to noise ratio, where a ratio of more than 4 is desirable [43]. In this study, the ratio observed for the model was found to be 56.4086, which indicates there is sufficient signal to navigate the design space.

Examination of the normal plot of residuals (**Figure 7a**) shows that the residuals are close to a straight line, implying that the errors are normally distributed and providing support that the terms in the model are significant. A graph of residual vs. predicted values is shown in **Figure 7b**. No unusual structure is visible. Since the standardized residuals are within the range, the proposed model is significant. Residuals vs. runs (**Figure 7c**) shows the order of the residuals from the experimental runs. This implies that the residuals are random and do not show any pattern with the order of trials. The residual vs sequence data image also shows that there is no discernible pattern or unusual structure in the data. This means that the proposed model is adequate and there is no reason to suspect a violation of the independence or constant variation assumptions. The Residuals vs Actuals (**Figure 7d**) is close to a straight line indicating that the data generated from the runs is more likely to be the data obtained from the experiments.

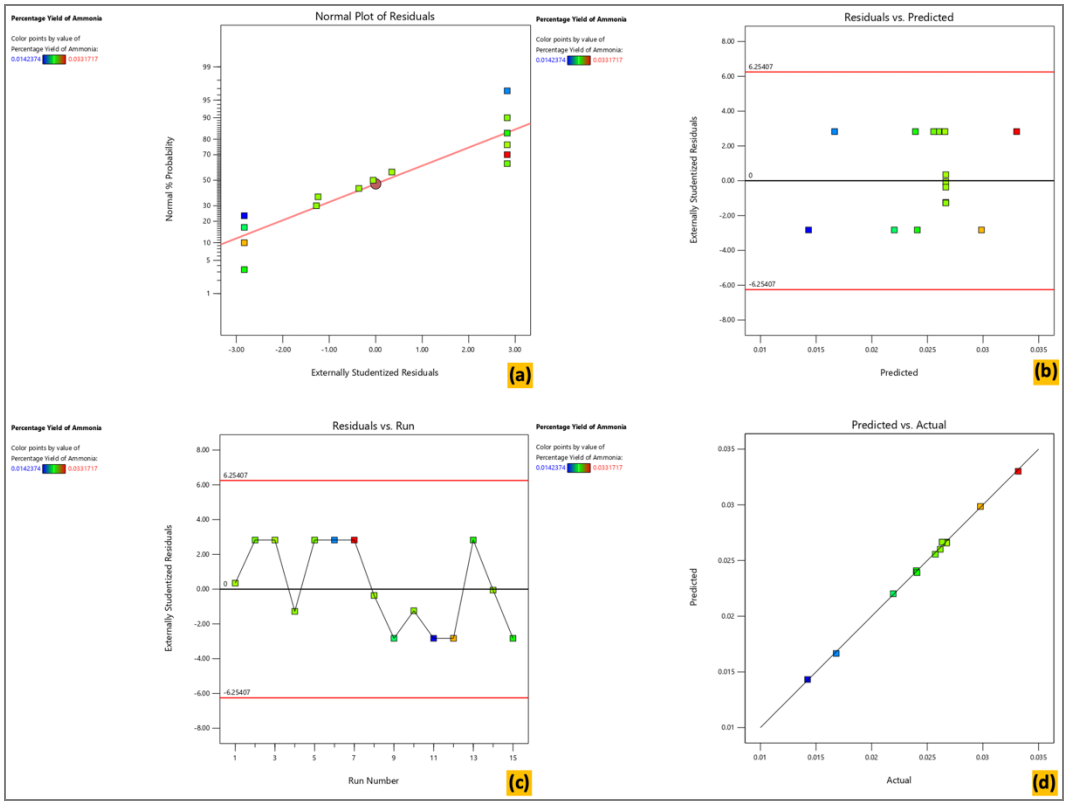


Figure 7. Distribution of data for percentage ammonia yield: (a) Normal probability plots; (b) Residuals vs. predicted; (c) Residuals vs. run; (d) Predicted vs actual

Figure 8 shows the 3D surface plot of percentage of ammonia yield at constant ammonia synthesis temperature (C) as a function of catalyst sintering temperature (A) and magnetic induction (B). Percentage of ammonia yield was found to increase in the early stage as shown in **Figure 8**, which then decreased as the catalyst sintering temperature and magnetic induction increased. The increase in ammonia yield at the initial stage was due to the positive effect of

magnetic induction and lower sintering temperature on the catalyst [44]. However, as the sintering temperature increased, the effectiveness of the catalyst decreased, which led to a decrease in ammonia yield [45]. Magnetic induction and catalyst composition play an important role in determining catalyst activity at various temperatures.

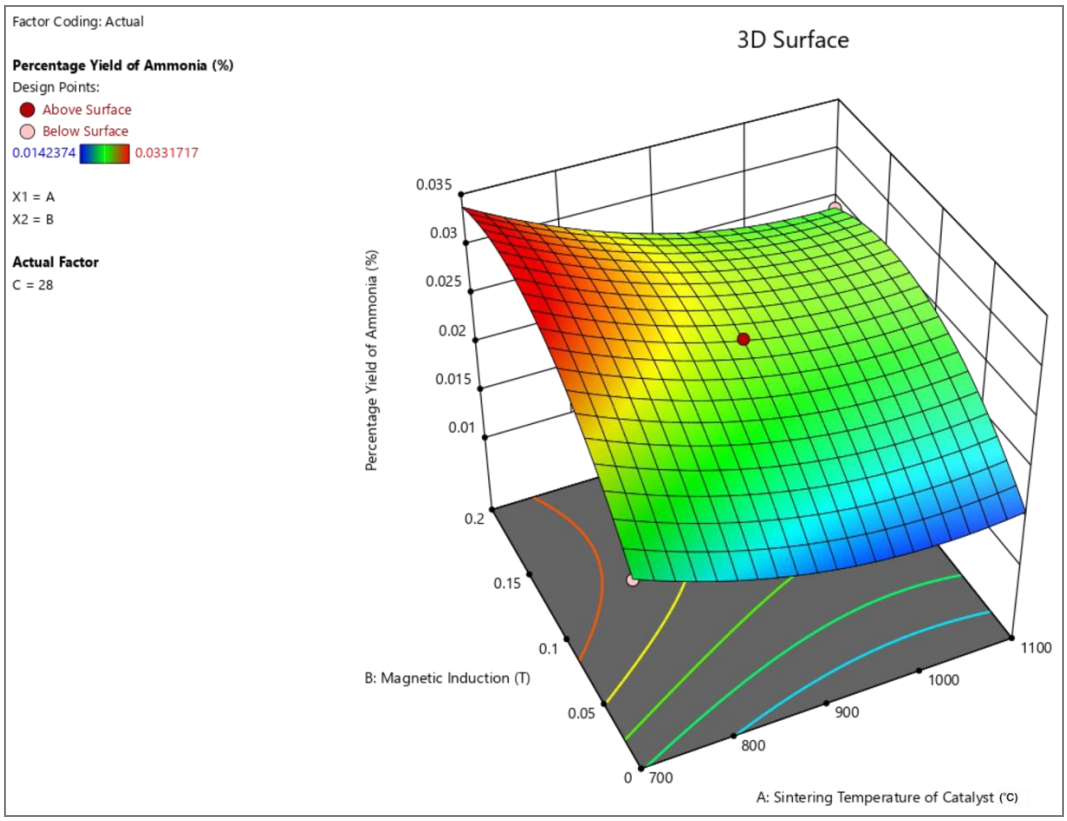


Figure 8. Combined effect of factors A-B on percentage of ammonia yield

Figure 9 shows the 3D surface plot of percentage of ammonia yield at constant magnetic induction (B) as a function of catalyst sintering temperature (A) and ammonia synthesis temperature (C). Percentage of ammonia yield was found to be high at the initial stage as shown in **Figure 9**, which then decreased as the catalyst sintering temperature and ammonia synthesis temperature increased. This is because at high temperatures, the exothermic reaction in ammonia synthesis tends to shift towards ammonia decomposition due to the law of thermal balance, which reduces ammonia yield [46]. Catalysts operated at high temperatures can increase the initial reaction rate, but further increases in temperature can lead to a decrease in yield due to increased ammonia decomposition [47]. At low to moderate temperatures, reaction kinetics are slower but thermodynamics are more favorable for ammonia formation [48].

Figure 10 shows the 3D surface plot of percentage of ammonia yield at constant catalyst sintering temperature (A) as a function of magnetic induction (B) and ammonia synthesis temperature (B). Percentage of ammonia yield was found to increase at an early stage as shown in **Figure 10**, which then decreased as the magnetic induction temperature and ammonia synthesis temperature increased. This is due to the increase in temperature which increases the rate of methanogenesis reaction. The increase in temperature from 25 °C to 35 °C doubles the rate constant of methanogenesis, which overcomes the effect of increased ammonia toxicity. Along with a further increase in temperature, the toxicity effect of high free ammonia concentration becomes more dominant, leading to a decrease in ammonia yield [49]. Magnetic fields also play an important role in this ammonia synthesis process, higher magnetic fields result in more effective catalytic activity and enhance the adsorption and desorption processes in ammonia synthesis [50].

3.4. Model Optimization and Validation

In the optimization analysis, the objective criterion was set as the minimum value for the catalyst sintering temperature and ammonia synthesis temperature factors, while for the magnetic induction factor, it was set in range and the maximum value was set for the dependent factor (Percentage of ammonia yield) as shown in **Table 8**. For the independent factors, the objective is to obtain the optimum value that will produce the optimum response as shown in **Figure 11**.

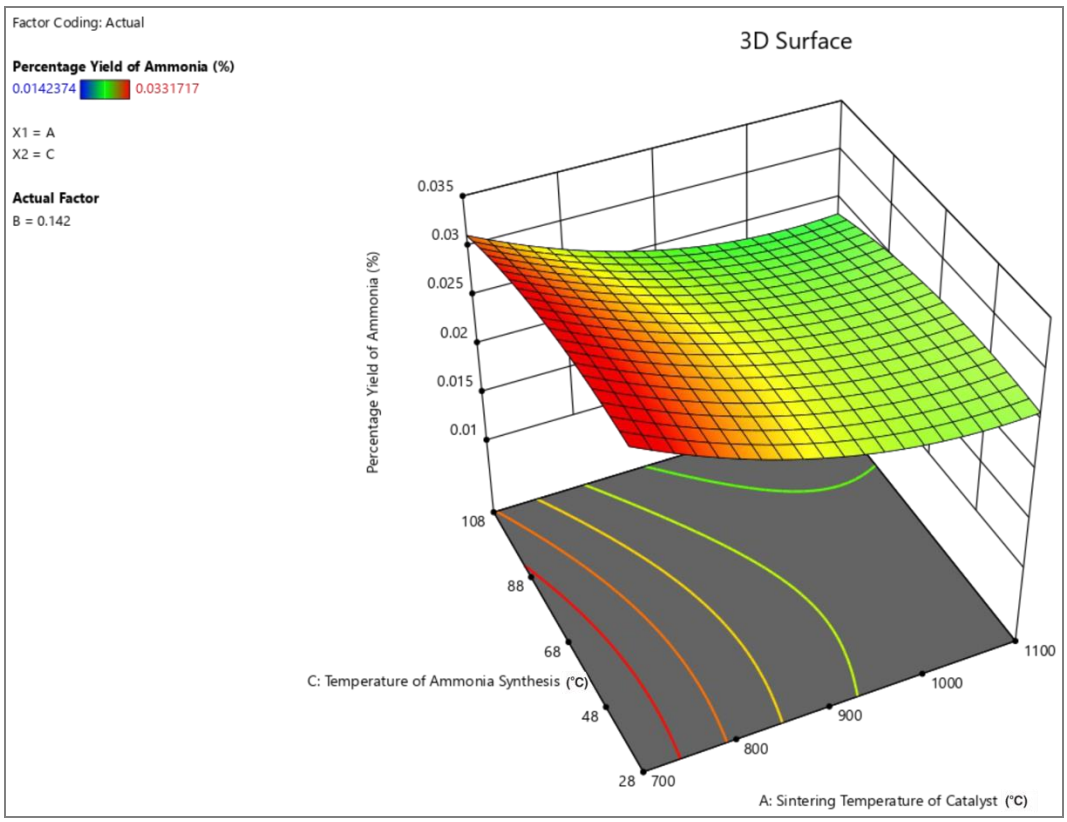


Figure 9. Combined effect of factors A-C on percentage of ammonia yield

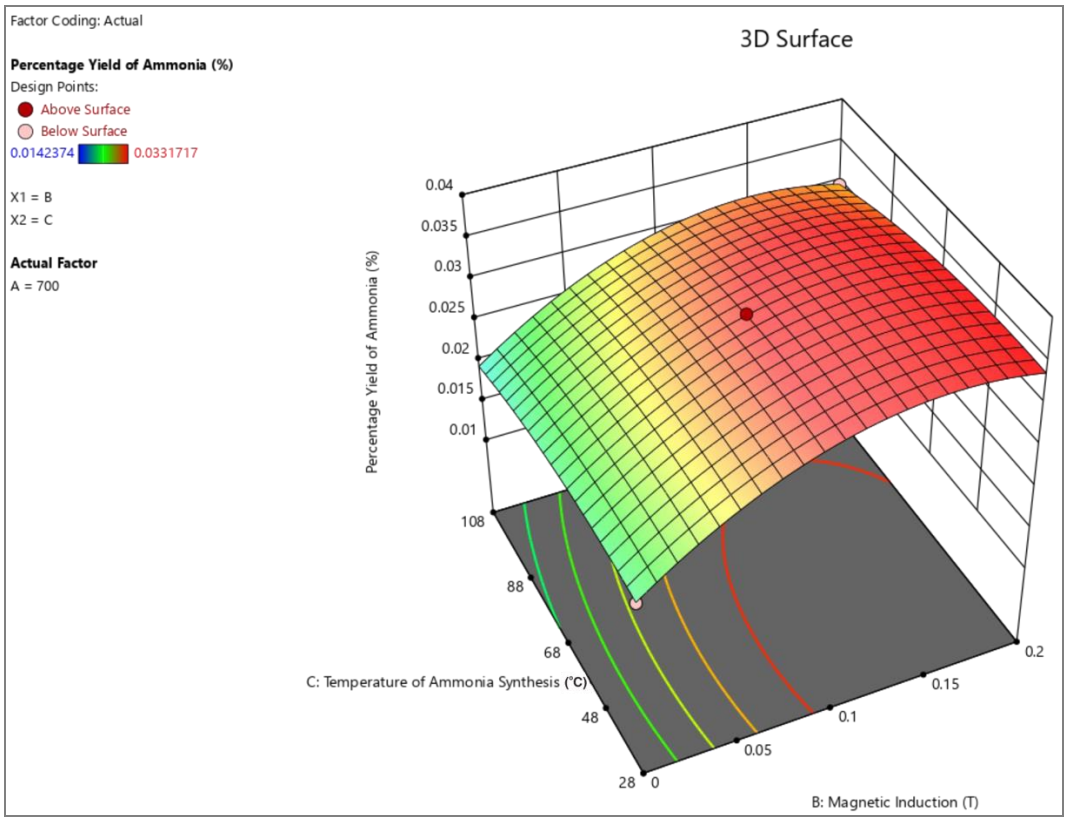


Figure 10. Combined effect of factors B-C on percentage of ammonia yield

Table 8. Validation of optimal response

Sintering Temperature of Catalyst [°C]	Magnetic Induction [T]	Temperature of Ammonia Synthesis [°C]	Percentage Yield of Ammonia [%]		
			Test 1	Test 2	Test 3
700	0.1422	28	0.0340546	0.0331259	0.0365476

Table 9. Confirmation of predicted response and optimal response

Solution 1 of 68 Response	Predicted Mean	Predicted Median	Std Dev	n	SE Pred	95% PI low	Data Mean	95% PI high
Percentage Yield of Ammonia	0.0347486	0.0347486	0.000276177	3	0.00055545	0.0333208	0.034576	0.0361765

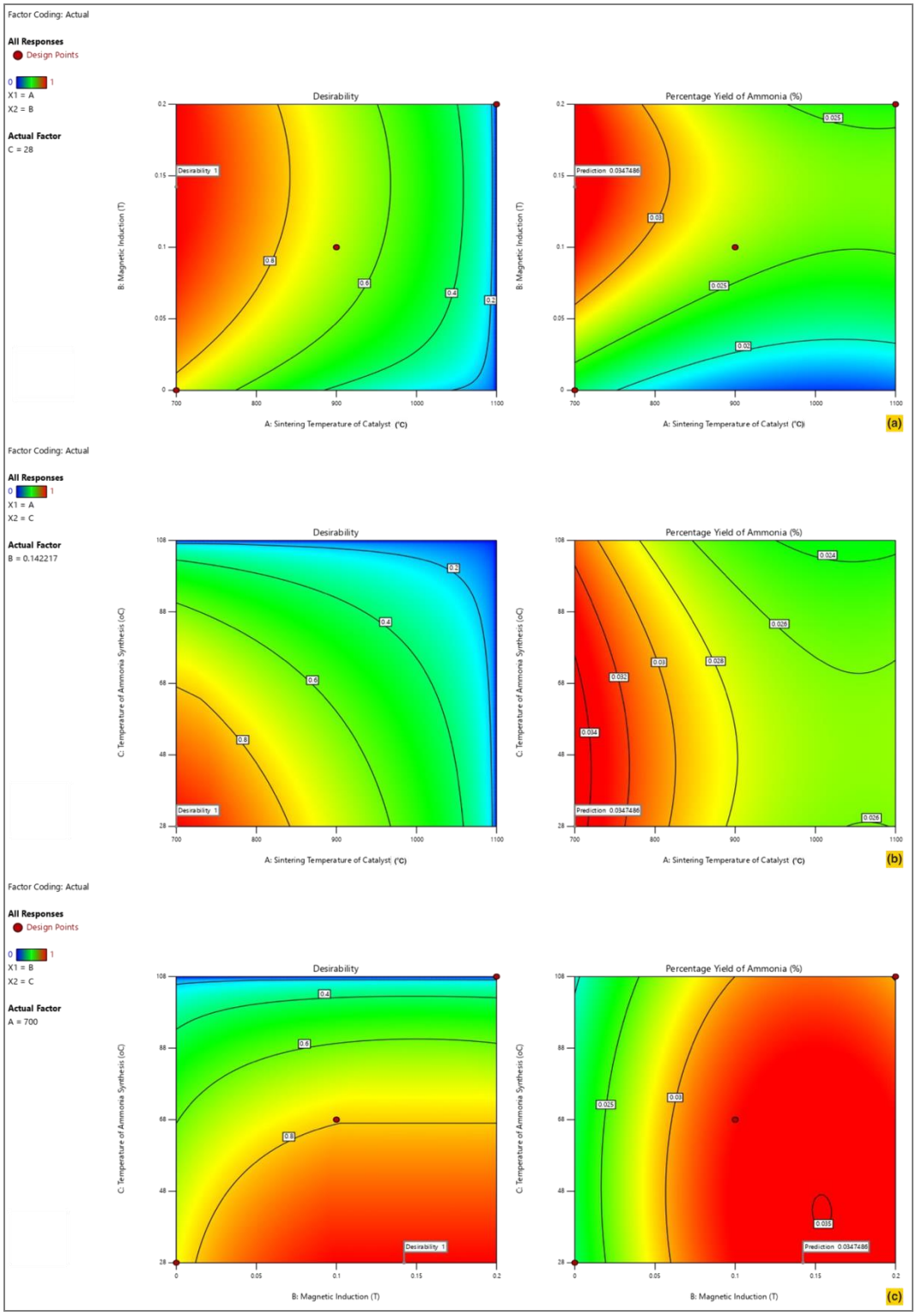


Figure 11.
2D graph of optimal response results for factors:
(a) A-B;
(b) A-C;
(c) B-C

Therefore, by applying the desirability function, the optimum response (Percentage of Ammonia Yield) was found to be 0.033 at 700 °C catalyst sintering temperature, 0.1422 T magnetic induction and 28 °C ammonia synthesis temperature with a good desirability of 1. At this optimum process condition, the difference between the predicted response (0.0347486%) and the experimental response (0.034576%) shows a very small value which indicates that the quadratic regression model is valid and accurate in predicting the response (Y) [41].

The high optimum Percentage of Ammonia Yield of 0.034576 is obtained at the minimum value of the factor, this is done to minimize the energy/source production of ammonia, where the higher the factor (catalyst sintering temperature, magnetic induction and ammonia synthesis temperature) will significantly increase the production cost of ammonia.

4. Conclusion

This study aims to investigate the use of $Mn_{0.8}Zn_{0.2}Fe_2O_4$ catalyst sintered with different temperatures, magnetic field induction and temperature during ammonia synthesis process, as well as the optimization of ammonia synthesis process using RSM and CCD methods. Therefore, some conclusions that can be drawn include:

- The crystallite size of the $Mn_{0.8}Zn_{0.2}Fe_2O_4$ sample increases as the sintering temperature increases.
- $Mn_{0.8}Zn_{0.2}Fe_2O_4$ has a sub-roundness morphology with high sphericity and agglomeration.
- The magnetic properties of $Mn_{0.8}Zn_{0.2}Fe_2O_4$ sintered at 700 °C and 900 °C have ferrimagnetic characteristics, while at 1100°C it has ferromagnetic characteristics.
- The highest reduction temperature of $Mn_{0.8}Zn_{0.2}Fe_2O_4$ catalyst was 788 °C in the 1100 °C sintering temperature. The hydrogen consumption for the three catalysts showed that the 700 °C $Mn_{0.8}Zn_{0.2}Fe_2O_4$ catalyst used most of the hydrogen.
- The synthesis of $Mn_{0.8}Zn_{0.2}Fe_2O_4$ catalyst using the Helmholtz coil method proved successful in forming ammonia in the form of NH_4OH and $(NH_4)_2SO_4$.
- Because the R^2 value reaches 99.73% and the residuals are normally distributed. It can be determined that the correlation between the input response and the output response, and the assumptions of the model are correct and the data is reliable.
- The most optimal parameters in the ammonia synthesis process are catalyst sintering temperature 700 °C, magnetic induction 0.1422 T, and ammonia synthesis temperature 28 °C. The validation between the predicted response and the experimental response based on the optimum conditions is very low, indicating that the quadratic regression model is valid and accurate in predicting the response.

Acknowledgements

The author would like to thank the State University of Malang for providing a grant under the Center for Excellence Research scheme with grant number 4.4.831/UN32.14.1/LT/2024.

Authors' Declaration

Authors' contributions and responsibilities - The authors made substantial contributions to the conception and design of the study. The authors took responsibility for data analysis, interpretation and discussion of results. The authors read and approved the final manuscript.

Funding – the State University of Malang under the Center for Excellence Research scheme with grant number 4.4.831/UN32.14.1/LT/2024.

Availability of data and materials - All data is available from the authors.

Competing interests - The authors declare no competing interests.

Additional information – No additional information from the authors.

References

[1] S. Giddey, S. P. S. Badwal, and A. Kulkarni, "Review of electrochemical ammonia production technologies and materials," *International Journal of Hydrogen Energy*, vol. 38, no. 34, pp. 14576–14594, Nov. 2013, doi: 10.1016/j.ijhydene.2013.09.054.

[2] H. Liu, *Ammonia Synthesis Catalysts: Innovation and Practices*. Singapore: World Scientific / Chemical Industry Press, China, 2013. doi: 10.1142/8199.

[3] A. Yapicioglu and I. Dincer, "A review on clean ammonia as a potential fuel for power generators," *Renewable and Sustainable Energy Reviews*, vol. 103, pp. 96–108, Apr. 2019, doi: 10.1016/j.rser.2018.12.023.

[4] J. N. Sahu, S. Hussain, and B. C. Meikap, "Studies on the hydrolysis of urea for production of ammonia and modeling for flow characterization in presence of stirring in a batch reactor using computational fluid dynamics," *Korean Journal of Chemical Engineering*, vol. 28, no. 6, pp. 1380–1385, Jun. 2011, doi: 10.1007/s11814-010-0524-9.

[5] P. Puspitasari, J. A. Razak, and N. Yahya, "Ammonia synthesis using magnetic induction

method (MIM)," in *AIP Conference Proceedings*, 2012, pp. 605–610. doi: 10.1063/1.4757543.

[6] S. H. Chien, L. I. Prochnow, S. Tu, and C. S. Snyder, "Agronomic and environmental aspects of phosphate fertilizers varying in source and solubility: an update review," *Nutrient Cycling in Agroecosystems*, vol. 89, no. 2, pp. 229–255, Mar. 2011, doi: 10.1007/s10705-010-9390-4.

[7] B. Azeem, K. KuShaari, Z. B. Man, A. Basit, and T. H. Thanh, "Review on materials & methods to produce controlled release coated urea fertilizer," *Journal of Controlled Release*, vol. 181, pp. 11–21, May 2014, doi: 10.1016/j.jconrel.2014.02.020.

[8] S. Sunaryo, S. Sutoyo, S. Suyitno, Z. Arifin, T. Kivevele, and A. I. Petrov, "Characteristics of briquettes from plastic pyrolysis by-products," *Mechanical Engineering for Society and Industry*, vol. 3, no. 2, pp. 57–65, Jun. 2023, doi: 10.31603/mesi.9114.

[9] W. Rarogpilecka *et al.*, "Carbon-supported ruthenium catalysts for NH3 synthesis doped with caesium nitrate: Activation process, working state of Cs–Ru/C," *Journal of Catalysis*, vol. 239, no. 2, pp. 313–325, Apr. 2006, doi: 10.1016/j.jcat.2006.01.035.

[10] N. Lashari and T. Ganat, "Emerging applications of nanomaterials in chemical enhanced oil recovery: Progress and perspective," *Chinese Journal of Chemical Engineering*, vol. 28, no. 8, pp. 1995–2009, Aug. 2020, doi: 10.1016/j.cjche.2020.05.019.

[11] M. A. Shipman and M. D. Symes, "Recent progress towards the electrosynthesis of ammonia from sustainable resources," *Catalysis Today*, vol. 286, pp. 57–68, May 2017, doi: 10.1016/j.cattod.2016.05.008.

[12] K. Ke, G. Wang, D. Cao, and G. Wang, "Recent Advances in the Electro-Oxidation of Urea for Direct Urea Fuel Cell and Urea Electrolysis," in *Electrocatalysis*, 2020, pp. 41–78. doi: 10.1007/978-3-030-43294-2_2.

[13] V. Polshettiwar and T. Asefa, *Nanocatalysis Synthesis and Applications*. Wiley, 2013. doi: 10.1002/9781118609811.

[14] P. Puspitasari and N. Yahya, "Development of ammonia synthesis," in *2011 National Postgraduate Conference*, IEEE, Sep. 2011, pp. 1–4. doi: 10.1109/NatPC.2011.6136449.

[15] S. Nazzal and M. A. Khan, "Response surface methodology for the optimization of ubiquinone self-nanoemulsified drug delivery system," *AAPS PharmSciTech*, vol. 3, no. 1, pp. 23–31, Mar. 2002, doi: 10.1208/pt030103.

[16] T. Damena and T. Alansi, "Review: Low Cost, Environmentally Friendly Humic Acid Coated Magnetite Nanoparticles (HA-MNP) and Its Application for the Remediation of Phosphate from Aqueous Media," *Journal of Encapsulation and Adsorption Sciences*, vol. 08, no. 04, pp. 256–279, 2018, doi: 10.4236/jeas.2018.84013.

[17] P. Puspitasar, N. Yahya, N. A. M. Zabidi, and N. A. Ahmad, "Comparison of Mechanical Properties and Magnetic Properties of Mn0.8Zn0.2Fe2O4 Synthesized by Conventional Ball Milling and Self Combustion Method," *Journal of Applied Sciences*, vol. 11, no. 7, pp. 1199–1205, Mar. 2011, doi: 10.3923/jas.2011.1199.1205.

[18] P. Puspitasari, A. Andoko, H. Suryanto, P. Risdanareni, and J. J. Ekaputri, "Properties of Mn 0.4 Zn 0.6 Fe 2 O 4 and Mn 0.6 Zn 0.4 Fe 2 O 4 as Nanocatalyst for Ammonia Production," *MATEC Web of Conferences*, vol. 97, p. 01029, Feb. 2017, doi: 10.1051/matecconf/20179701029.

[19] K. H. Tshai, N. Yahya, F. K. Chong, and V. V. Yap, "Optimization of green synthesis of ammonia by magnetic induction method using response surface methodology," in *3rd International Conference on Fundamental and Applied Sciences (ICFAS 2014): Innovative Research in Applied Sciences for a Sustainable Future*, 2014, pp. 223–230. doi: 10.1063/1.4898470.

[20] A. A. Bunaciu, E. gabriela Udriştioiu, and H. Y. Aboul-Enein, "X-Ray Diffraction: Instrumentation and Applications," *Critical Reviews in Analytical Chemistry*, vol. 45, no. 4, pp. 289–299, Oct. 2015, doi: 10.1080/10408347.2014.949616.

[21] D. D. Pramono and P. Puspitasari, "Comparison of physicochemical properties of hydroxyapatite from scallop shell synthesized by wet chemical method with and without sonication process," in *Proceedings of the International Conference on Green Engineering & Technology 2022 (IConGETech 2022)*, Arau: AIP Conference Proceedings, 2024, p. 040034. doi: 10.1063/5.0199107.

[22] S. H. Jaafar *et al.*, "Influence of Calcination Temperature on Crystal Growth and Optical Characteristics of Eu3+ Doped ZnO/Zn2SiO4 Composites Fabricated via Simple Thermal Treatment Method," *Crystals*, vol. 11, no. 2, p. 115, Jan. 2021, doi: 10.3390/cryst11020115.

[23] V. Lakshmi Narayana and L. Bhaskara Rao, "A brief review on the effect of alkali treatment on mechanical properties of various natural fiber reinforced polymer composites," *Materials Today: Proceedings*, vol. 44, pp. 1988–1994, 2021, doi: 10.1016/j.matpr.2020.12.117.

[24] A. A. Mirzaei, H. R. Shaterian, S. H. Taylor, and G. J. Hutchings, "Co-precipitated Copper Zinc Oxide Catalysts for Ambient Temperature Carbon Monoxide Oxidation: Effect of Precipitate Aging Atmosphere on Catalyst Activity," *Catalysis Letters*, vol. 87, no. 3–4, pp. 103–108, Apr. 2003, doi: 10.1023/A:1023416819195.

[25] M. A. Gabal *et al.*, "Recovery of Mn0.8Zn0.2Fe2O4 from Zn–C battery: auto-combustion synthesizes, characterization, and electromagnetic properties," *Journal of Sol-Gel Science and Technology*, vol. 100, no. 3, pp. 526–537, Dec. 2021, doi: 10.1007/s10971-021-05608-9.

[26] Y. Liu, S. Zhu, Z. Gu, C. Chen, and Y. Zhao, "Toxicity of manufactured nanomaterials," *Particuology*, vol. 69, pp. 31–48, Oct. 2022, doi: 10.1016/j.partic.2021.11.007.

[27] C. B. Carter and M. G. Norton, *Ceramic Materials*. New York, NY: Springer New York, 2013. doi: 10.1007/978-1-4614-3523-5.

[28] W. D. Callister and D. G. Rethwisch, *Materials science and engineering: an introduction*, vol. 9. Wiley New York, 2018.

[29] C. Chacon and O. Isnard, "Crystal and magnetic structure of YCo4−xFexB," *Journal of Applied Physics*, vol. 89, no. 1, pp. 71–75, Jan. 2001, doi: 10.1063/1.1331067.

[30] Z. Luo *et al.*, "Effect of sintering temperature on microstructure and magnetic properties for Fe-Si soft magnetic composites prepared by water oxidation combined with spark plasma sintering," *Journal of Magnetism and Magnetic Materials*, vol. 491, p. 165615, Dec. 2019, doi: 10.1016/j.jmmm.2019.165615.

[31] M. D. Nguyen, H.-V. Tran, S. Xu, and T. R. Lee, "Fe3O4 Nanoparticles: Structures, Synthesis, Magnetic Properties, Surface Functionalization, and Emerging Applications," *Applied Sciences*, vol. 11, no. 23, p. 11301, Nov. 2021, doi: 10.3390/app112311301.

[32] Q. Tang and K. Huang, "Determining the kinetic rate constants of Fe3O4-to-Fe and FeO-to-Fe reduction by H2," *Chemical Engineering Journal*, vol. 434, p. 134771, Apr. 2022, doi: 10.1016/j.cej.2022.134771.

[33] T. P. Almeida, M. W. Fay, Y. Zhu, T. W. Hansen, R. Dunin-Borkowski, and P. D. Brown, "Environmental TEM investigation of the reduction of α-Fe 2 O 3 nanorods under H 2 atmosphere," *Journal of Physics: Conference Series*, vol. 371, p. 012049, Jul. 2012, doi: 10.1088/1742-6596/371/1/012049.

[34] J. Li, J. Gao, X. Wang, Y. Guo, and F. Cheng, "Spinel Ferrite Transformation for an Efficient Fe Removal from Circulating Fluidized Bed Fly Ash by Carbothermal Reduction at a Low Temperature," *ACS Omega*, vol. 7, no. 22, pp. 18612–18622, Jun. 2022, doi: 10.1021/acsomega.2c01277.

[35] J. Marugán, J. A. Botas, M. Martín, R. Molina, and C. Herradón, "Study of the first step of the Mn2O3/MnO thermochemical cycle for solar hydrogen production," *International Journal of Hydrogen Energy*, vol. 37, no. 8, pp. 7017–7025, Apr. 2012, doi: 10.1016/j.ijhydene.2011.10.124.

[36] R. Findorák *et al.*, "Experiments and Simulations on the Low-Temperature Reduction of Iron Ore Oxide Pellets with Hydrogen," *Metals*, vol. 15, no. 3, p. 289, Mar. 2025, doi: 10.3390/met15030289.

[37] X. Xu *et al.*, "Size-Dependent Reduction Kinetics of Iron Oxides in Single and Mixed Mineral Systems," *Environmental Science & Technology*, vol. 59, no. 5, pp. 2519–2530, Feb. 2025, doi: 10.1021/acs.est.4c08032.

[38] J. M. Bellosta von Colbe *et al.*, "Scale-up of milling in a 100 L device for processing of TiFeMn alloy for hydrogen storage applications: Procedure and characterization," *International Journal of Hydrogen Energy*, vol. 44, no. 55, pp. 29282–29290, Nov. 2019, doi: 10.1016/j.ijhydene.2019.01.174.

[39] V. Bansal, C. Bansal, and S. K. Dhawan, "Charge transport and ammonia sensing response in poly (aniline-co-1-amino-2-naphthol-4-sulphonic acid)," *Indian Journal of Engineering & Materials Sciences*, vol. 16, pp. 355–363, 2009.

[40] M. Kumari and S. K. Gupta, "Removal of aromatic and hydrophobic fractions of natural organic matter (NOM) using surfactant modified magnetic nanoadsorbents (MNPs)," *Environmental*

Science and Pollution Research, vol. 25, no. 25, pp. 25565–25579, Sep. 2018, doi: 10.1007/s11356-018-2611-0.

[41] J. Bayuo, B. Kenneth, and A. A. Moses, "Optimization of Adsorption Parameters for Effective Removal of Lead (II) from Aqueous Solution," *Physical Chemistry: An Indian Journal*, vol. 14, no. 1, 2019, [Online]. Available: http://www.tsijournals.com

[42] D. Nahemiah, I. Nkama, and B. Mamudu, "Application of Response Surface Methodology (RSM) and Central Composite Design (CCD) to Optimize Minerals Composition of Rice-Cowpea Composite Blends during Extrusion Cooking," *International Journal of Food Science and Nutrition Engineering*, vol. 5, no. 1, pp. 40–52, 2015, doi: 10.5923/j.food.20150501.06.

[43] M. Kumari and S. K. Gupta, "Response surface methodological (RSM) approach for optimizing the removal of trihalomethanes (THMs) and its precursor's by surfactant modified magnetic nanoadsorbents (sMNP) - An endeavor to diminish probable cancer risk," *Scientific Reports*, vol. 9, no. 1, p. 18339, Dec. 2019, doi: 10.1038/s41598-019-54902-8.

[44] J. A. Razak, S. Sufian, K. Z. Ku Shaari, P. Puspitasari, T. K. Hoe, and N. Yahya, "Synthesis, characterization and application of Y[sub 3]Fe[sub 5]O[sub 12] nanocatalyst for green production of NH[sub 3] using magnetic induction method (MIM)," in *International Conference on Fundamental and Applied Sciences 2012: (ICFAS2012)*, 2012, pp. 633–638. doi: 10.1063/1.4757548.

[45] Ł. Czekajło and Z. Lendzion-Bieluń, "Wustite based iron-cobalt catalyst for ammonia synthesis," *Catalysis Today*, vol. 286, pp. 114–117, May 2017, doi: 10.1016/j.cattod.2016.11.013.

[46] X. Li, X. Zhang, H. O. Everitt, and J. Liu, "Light-Induced Thermal Gradients in Ruthenium Catalysts Significantly Enhance Ammonia Production," *Nano Letters*, vol. 19, no. 3, pp. 1706–1711, Mar. 2019, doi: 10.1021/acs.nanolett.8b04706.

[47] Y. Ogura *et al.*, "Efficient ammonia synthesis over a Ru/La 0.5 Ce 0.5 O 1.75 catalyst pre-reduced at high temperature," *Chemical Science*, vol. 9, no. 8, pp. 2230–2237, 2018, doi: 10.1039/C7SC05343F.

[48] V. Kyriakou, I. Garagounis, E. Vasileiou, A. Vourros, and M. Stoukides, "Progress in the Electrochemical Synthesis of Ammonia," *Catalysis Today*, vol. 286, pp. 2–13, May 2017, doi: 10.1016/j.cattod.2016.06.014.

[49] M. L. Garcia and L. T. Angenent, "Interaction between temperature and ammonia in mesophilic digesters for animal waste treatment," *Water Research*, vol. 43, no. 9, pp. 2373–2382, May 2009, doi: 10.1016/j.watres.2009.02.036.

[50] N. Yahya, P. Puspitasari, and N. H. Noordin, "Ammonia Synthesis Using Magnetically Induced Reaction," *Defect and Diffusion Forum*, vol. 334–335, pp. 329–336, Feb. 2013, doi: 10.4028/www.scientific.net/DDF.334-335.329.